HIGH SCHOOL EDITION
Journal of Student Research
Volume 12 Issue 1 (2023)

Detection of Reactive Oxygen Species during Photodynamic Therapy

Dipakshi Pal[1] and Dr. Aniruddha Ray[2#]

[1]Sylvania Northview High School, 5403 Silica Drive, Sylvania, Ohio, 43560, U.S.A.
[2]University of Toledo
[#]Advisor

ABSTRACT

Reactive oxygen species (ROS), also known as oxidants, are often utilized in a variety of therapies, such as in photodynamic therapy (PDT) which is an emergent cancer and tumor therapy. The production of ROS in cancerous cells induces oxidative stress, promoting apoptotic cell death. Here we utilize fluorescent molecular sensors to quantify the generation of ROS by a photosensitizer and a room-temperature plasma source. We observe a linear increase in the production of ROS in solution, as a function of light irradiation dose, as measured by the intensity of fluorescence of sensor molecules. The same trend was also observed using the plasma source. It was also observed that in both experiments the signal saturated after prolonged irradiation time. This can be attributed to finite concentration of sensor molecules present in the solution. While ROS production can continue to increase linearly due to further irradiation, the increase in ROS can no longer be detected after prolonged irradiation time due to the limited number of sensors in the sample.

1. INTRODUCTION

Cancer is one of the leading causes of death worldwide with 9.5 million cancer-related deaths and 18.1 million new cases of cancer being diagnosed in 2018 (National Cancer Institute, 2021). Furthermore, these numbers are expected to rise every year, and it is predicted that by 2040, the number of new cancer cases will rise to 29.5 million cases and the number of cancer-related deaths will rise to 16.4 million (National Cancer Institute, 2021). Cancer by definition is the continuous abnormal growth and unhealthy reproduction of mutated cells in the body which can result in invasion to nearby tissues and migration to distant parts of the body. This can deprive the body's healthy cells of their necessary nutrients, leading to organ failure, and ultimately death (Visone, 2010). In total, there are over 100 different types of cancer, leading to the need for innovative and specific treatment plans for each unique cancer type (National Cancer Institute, 2021). Due to the large population of people diagnosed with malignancies, it is crucial to explore different treatment modalities to improve the health and quality of life of cancer patients.

Today, there are many different treatments for cancer. The most commonly used cancer therapy today is chemotherapy, which is the treatment of cancer cells through the use of different drugs to target and eliminate the living, remaining cancer cells (Sekar, 2014). The different drugs used for chemotherapy results in numerous side effects such as nausea and vomiting, diarrhea, transient hair loss, excessive bleeding, shortness of breath, dizziness, excessive fatigue, numbness, and jaundice (Islam, 2019).

However, an alternate treatment to chemotherapy is photodynamic therapy. This is a rising treatment for cancer that utilizes light and specialized drugs called photosensitizing drugs to destroy cancer cells (Photodynamic therapy (PDT), 2021). The light is the activator in this treatment to initiate a chemical reaction that destroys the harmful cells (Photodynamic therapy (PDT), 2021). This is performed by encouraging the production of oxidants within the cells to promote apoptosis, or programmed cell death (Elmore, 2007). These oxidants, also known as reactive oxygen species or "ROS," are an important part of this cancer treatment. There are many different forms of ROS, such

as singlet oxygen, hydroxyl radical, hydrogen peroxide amongst others. Singlet oxygen is a highly reactive form of oxygen that attacks and breaks apart almost every organic molecule it encounters (Photodynamic therapy (PDT), 2021). Thus, the production of singlet oxygen, in cells is effective in photodynamic therapy because when produced within the cell, they can break down the specific, targeted cells from the inside (Elmore, 2007). In photodynamic therapy, the reactive oxygen species are produced by the photosensitizers. When illuminated with their excitation wavelength, the photosensitizers present in the cell initiate a chemical reaction which produces ROS (Photodynamic therapy (PDT), 2021). This production of ROS in cells ultimately leads the cells to undergo apoptosis due to the destructive nature of ROS. Therefore, ROS is the building block of the entirety of photodynamic therapy.

Additionally, this form of therapy on cancers today is specifically applicable to small tumors in skin, head, neck, and oral cancers and may have future applications for cancer treatment (Photodynamic Therapy for Cancer, 2021). Another therapy that relies on the generation of ROS is plasma therapy, which uses highly ionized gases. Plasma discharge is used for disinfection purpose and has been under heavy research for cancer treatment as well (Harley, 2022).

This research focuses on modeling and detecting the amount (ROS) produced during photodynamic therapy and plasma therapy. It is necessary to understand the quantity of oxidants that are produced through the photodynamic reaction so that photodynamic therapy can be used to target the specific tumors and avoid harming normal, healthy cells. The production of excessive oxidants in an area in the body can result in the destruction of nearby tissues can be more harmful overall. Moreover, insufficient production of ROS may lead to failure of therapy. Thus, quantification of the dose dependent ROS production will help optimize PDT and other treatments that rely on ROS production.

2. METHODS

Since the focus of this project is specifically the detection of ROS during photodynamic therapy, I conducted two experiments simulating this process in a similar fashion as the same method and technics it would be administered for patients in the lab.

The process of photodynamic therapy includes two main elements: the photosensitizer and energy (usually light energy). In this therapy, the photosensitizer is responsible for the creation of ROS. This is made possible when the photosensitizer is provided energy (such as being shined with light), causing it to undergo a chemical reaction which ultimately produces ROS.

In addition to these two elements involved in photodynamic therapy, in my experiments I also included a third component: photosensors. Photosensors are known to be originally non-fluorescent molecules that become fluorescent once they react with ROS. The addition of photosensors were critical in the detection of the production of ROS.

3. EXPERIMENT 1: Solution of RB in DMSO and DHR

To perform this first experiment of PDT and ROS detection, the experiment was conducted with solutions of Rose Bengal (RB) in Dimethyl Sulfoxide (DMSO) and Dihydrorhodamine (DHR) were mixed and then illuminated with light of wavelength range ~542–582 nm (under the TXR (red) filter).

For this experiment, RB dye is used as the photosensitizer, meaning that generates ROS when excited by light. To quantify the amount of ROS produced DHR dye was used as a sensor molecule. DHR is a non-fluorescent molecule and when oxidized by these oxidants, exhibits bright fluorescence.

The TXR (red) filter is used for irradiation because the peak wavelength for excitation of Rose Bengal is 559 nm which is within this filter's excitation bounds of 542-582 nm. Utilizing this filter where the excitation wavelength for the photosensitizer falls withing the boundary of the filter allows for precise, clear images of the sample to be able to be taken.

3.1 Preparation of Rose Bengal (RB) in Dimethyl sulfoxide (DMSO)

For the photosensitizer, RB was used since it is a common molecular photosensitizer compound implemented in photodynamic therapy for patients and has also been used in various experiments regarding photodynamic therapy such as in breast cancer lines (Atenco-Cuautle, 2019). The preparation of the photosensitizer for the first experiment is fundamental to replicate photodynamic therapy. For the photosensitizer, RB was used since it is a common molecular photosensitizer compound implemented in photodynamic therapy for patients and has also been used in various experiments regarding photodynamic therapy such as in breast cancer lines (Atenco-Cuautle, 2019).

Additionally, since the RB dye is originally in a solid state, for simplicity in the experiment it was dissolved in dimethyl sulfoxide, which is a widely used solvent in science laboratories (Dimethyl sulfoxide, 2021). Dissolving the RB dye in DMSO allowed for the photosensitizer of RB to become a solution, which is necessary for the experiment later.

The stock solution of RB in DMSO is much higher than the desired concentration. To lower this initial concentration of RB down to a desired concentration of 10 μM, a dilution is performed using distilled water. The dilution is conducted using the values calculated from M1V1=M2V2, where M denotes molarity (concentration) and V represents volume.

After the initial combination and mixture of RB and DMSO using stock solutions, the concentration of this mixture comes out to be much higher than the desired concentration. To lower this initial concentration of RB and DMSO down to a desired concentration of 10 μM, a dilution is performed using distilled water. The dilution is conducted using the values calculated from M1V1=M2V2, where M denotes molarity (concentration) and V represents volume.

In this experiment, I dissolved 1 milligram of solid Rose Bengal in 8 milliliters of distilled water to prepare a 102.7 μM solution of RB in DMSO. Then, I diluted this solution down to 10 μM by adding 903 μL of distilled water to 97.4 μL of the 102.7 μM solution of RB in DMSO. These exact numbers were calculated using the equation M1V1=M2V2, where M1 = 102.7 μM and M2 = 10 μM.

This determination of the concentration of RB dissolved in DMSO to use 10 μM for the experiment was reached through a series of trial and error while conducting this experiment previously. Finally, this concentration was chosen since it allowed for the images to be able to be analyzed with enough time intervals (as seen later on).

3.2 Preparation of Dihydrorhodamine (DHR)

Dihydrorhodamine, also known as DHR, is used in this experiment as the photosensor. DHR follows the definition of a photosensor as it is initially a non-fluorescent molecule that only becomes fluorescent after binding to ROS (Dihydrorhodamine 123, 2021). DHR was chosen for this experiment since it is a very easily and quickly oxidized by ROS and due to its characteristic qualities of a photosensor.

Since the stock solution DHR comes as a liquid, this liquid stock solution of DHR was simply prepared for this experiment by diluting it down to the desired concentration of 5 μM using distilled water. To complete this dilution, the amount of water needed is calculated through the dilution equation of M1V1=M2V2, where M denotes molarity (concentration) and V represents volume.

3.3 Mixture

After the preparation of the photosensitizers and photosensors of RB in DMSO and DHR respectively, the two components are mixed in equal proportions. In my trials, I mixed 100 μL of the 10 μM of RB in DMSO solution and 100 μL of the 5 μM solution of DHR.

After adding the two solutions together, they are vortexed. This is important to execute as it will help disperse the molecules of photosensors and photosensitizers evenly through the sample so that the illumination and imaging of the sample is consistent throughout. Once this is completed, the sample is prepared and ready for subsequent experimentation.

3.4 Microscope and Illumination

The LasX software was used along with a fluorescence microscope to image the sample of 200 µL RB in DMSO and DHR. First, the vial that included the samples of photosensors and photosensitizers prepared in the last few steps was placed under the microscope and moved into the center of the imaging field and focused under the phase contrast mode.

After the sample was focused, the microscope was switched to fluorescence mode, and the color of fluorescence was changed to green. An image of the capillary was then taken under the FTC (green) filter using the LasX program. This specific filter was used since it was corresponding wavelength of light that would allow for the imaging of the fluorescence from the photosensors within the sample.

Next, a calibration of the exposure for the images was performed. An image of the sample was taken under the FTC (green) filter and the exposure on the LasX software was calibrated to be completely black and was noted down to be used for subsequent images. The necessity for this calibration was to be able to base the subsequent images taken, and their resulting fluorescence to be able to analyze for the amount of photosensors that became active through the illumination. Making the "zero" illumination time completely black with zero fluorescence allowed for a baseline measurement. This calibrated imaged was then renamed as "0 seconds" for the illumination time.

After this, the microscope was then changed to the TXR (red) filter, and the sample was illuminated for 2 seconds. After illuminating for 2 seconds, the microscope was changed back to the FITC (green) filter, and an image was taken using the calibrated exposure and gain. This image was then renamed with its illumination time (ex. "2 seconds") and saved.

This process of illuminating the capillary under the TXR (red) filter was repeated in 2 seconds intervals, following by imaging under the FTC (green) filter with the same calibrated exposure and gain until saturation of fluorescence intensity. All the images were saved to the computer with their corresponding names as the illumination time under the TXR (red) filter.

The solution was illuminated with the TXR (red) filter because the wavelength of the light under the TXR (red) filter initiates the production of ROS within the capillary sample because it matches with the excitation wavelength of the photosensitizer (RB in DMSO) to encourage the production of ROS. The produced ROS from the illumination of the photosensitizers in the sample is then used to bind to the photosensors (DHR) in the solution. This is what causes the sample to become fluorescent for image analysis.

3.3 Image Analysis

The ImageJ software was utilized in analyzing the images taken by the microscope which was performed at the last state of the experiment. Each image is dragged into the ImageJ application, and then the image is analyzed to calculate the mean intensity of the highlighted segment. This analysis through the program is repeated for all the images taken of the capillary.

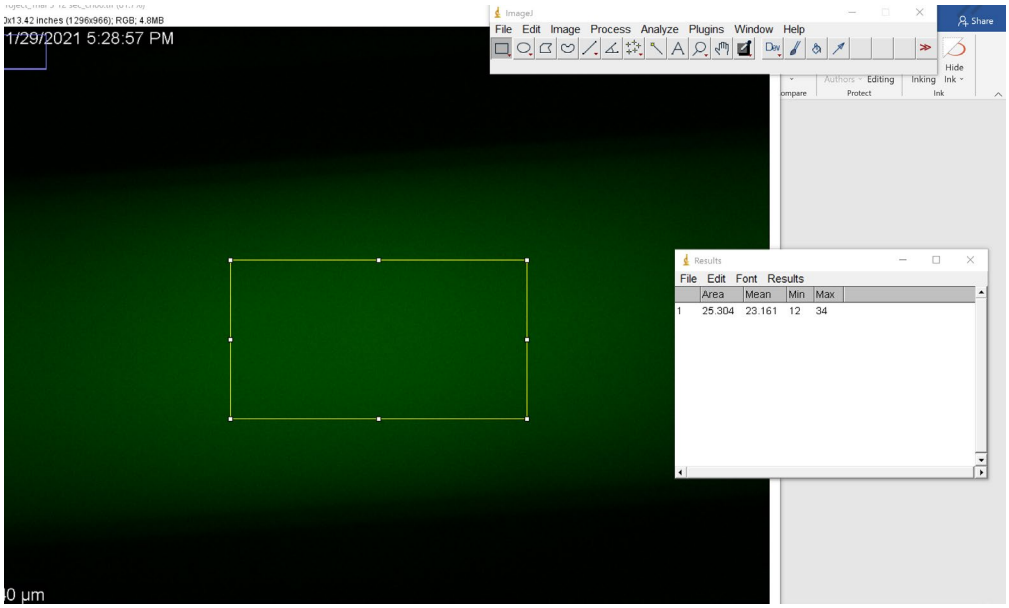

Figure 1: ImageJ View

In the exported spreadsheet of results from ImageJ, the output values include the area of the highlighted portion of the image, the mean intensity value, and the maximum and minimum intensity values. To create the graph to model the amount of ROS produced using the intensity of the sample, through the data labelled "mean" in the ImageJ software, which is the average intensity of the highlighted portion of the image of the illuminated capillary, the average intensity is calculated by:

$$\int_{i=min}^{i=max} (Intensity)di \,/\, \int_{a=min}^{a=max} (Area)da$$

Where, I = Intensity, di = ΔIntensity, A = Area, da = ΔArea

For each image, the average intensity of the image was matched to the corresponding time of illumination for the image and is recorded in a table. The time is the independent variable, and the intensity is the dependent variable. A graph of intensity vs. time was then generated.

The mean intensity of the images to model the production of ROS was used due to how the experiment was structured utilizing photosensors. The photosensor used in this experiment is DHR, which emit a green fluorescence once they bind with ROS molecules. The production of ROS in the sample can modeled using the mean intensity measurement from ImageJ. The larger the number of photosensors that bind with ROS, the greater the fluorescence, measured by the mean intensity of the image. Thus, analyzing the mean intensity of the images reveal the general trend of the production of ROS with time.

4. EXPERIMENT 2: Nanoparticles

Poly (lactic-co-glycolic acid) (PLGA) is one of the most effective biodegradable polymeric nanoparticles (NPs). It has been approved by the US FDA to use in drug delivery systems due to controlled and sustained- release properties, low toxicity, and biocompatibility with tissue and cells (Sadat Tabatabaei, 2021). Singlet oxygen sensor green (SOSG) is a detection reagent that is highly selective for singlet oxygen (Sadat Tabatabaei, 2021).

In this experiment, SOSG fluorescent dye encapsulated PLGA nanoparticles were irradiated using a plasma source. SOSG encapsulated PLGA nanoparticles were suspended in water and irradiated with plasma source to produce singlet oxygen. The SOSG dye gets oxidized by singlet oxygen, and thus nanoparticles become fluorescent.

This second experiment was chosen to be executed since in medical applications nanoparticles are a better alternative to the molecular methods such as what was used in experiment 1. Due to the characteristics of nanoparticles, precisely their "solubility, early degradation, and biodistribution" (Gelperina, 2005), nanoparticles have been seen to be more effective in penetration within cells and cancer cell uptake (Gelperina, 2005). Both experiments are fundamental to understanding the creation of ROS during therapy.

4.1 Preparing the Nanoparticle Solution

The previously prepared SOSG encapsulated nanoparticles were first collected in one vial, and subsequently, distilled water was added to the vial so that the total volume of nanoparticles adds up to 250 µL. The water is added so the concentration of nanoparticles can be lowered, as well as the water will help in breaking clusters of nanoparticles when sonicating in the next step.

The vial of the prepared nanoparticles dispersed throughout water was then sonicated in the middle of the sonicator. This is performed because the middle of the sonicator is where the maximum vibrations occur. The vial is sonicated for about 300 seconds in the sonicator. Sonicating the nanoparticles in distilled water will break any clusters of nanoparticles, which will help to avoid the overlap of the fluorescence signal (saturation) during imaging and analysis.

4.2 Preparing the Slides

To prepare slides to place the nanoparticles on, 5 new and precleaned glass slides were taken and placed on a sterilized paper towel. Then, each slide is labelled as 0 s, 10 s, 20 s, 30 s, and 40 s. Next, on each slide 33 µL of the nanoparticle solution was dropped into the middle of the slide using the pipette. This value of 33 µL was used because it was calculated to be the volume of solution that can be placed on a slide without overflowing over the edge.

4.3 Irradiation

Originally, this experiment was attempted to be conducted using irradiation under a light filter, but the reaction took too long to be observed for analysis. Therefore, I utilized the usage of plasma, due to its implementation in a similar therapy that relies on the generation of ROS called plasma therapy. In this therapy, plasma discharge is considered to be in future be very regularly used for cancer treatment through the production of ROS, like in photodynamic therapy (Harley, 2021).

The energy for the oxidation reaction within the photosensitizers in this experiment was provided through a plasma source. Plasma is used as the method to provide energy here since plasma beholds a huge sum of energy. The large amount of energy provided by the plasma allows the reaction to be much more targeted and at a significantly faster rate as compared to a light filter.

First, to provide the samples with plasma, the plasma source was plugged into the wall and powered on. Then, a specific height was set from which the plasma will be treated to the slides at a constant rate to avoid adding any other variables to the experiment. It was important that this height is constant because if the height was changed, different amounts of energy would be added to different slides. This would cause inconsistent data findings, and therefore it was crucial to avoid this potential error.

Then at this specific height the amount of plasma irradiated on that slide was respective for each slide with its label of time. For example, the slide labeled "10 s," was irradiated with plasma for exactly 10 seconds.

Based on the labeled time on each slide, the area of nanoparticle solution was irradiated with plasma for the designated time at the height previously set. After irradiation for each slide, the slide was placed to the side to dry. Once all the slides are completely dry after irradiation, which means there is no more liquid remaining on the slide's surface, the slides were ready to be imaged.

4.4 Microscope and Imaging

Like Experiment 1, the LasX software was used to image the samples. Once the software and microscope were turned on, the slide with 0 seconds of irradiation was placed into the microscope. Then, the sample was focused on the middle of the microscope in phase contrast mode with very low exposures and gains to avoid any extra irradiation of the nanoparticles.

Then, the microscope was changed to the fluorescence mode and the FITC (green) filter was selected (because the excitation wavelength of SOSG dye is 480 nm) to take images of the samples. Similar to Experiment 1, the exposure and gain for this 0-second slide were calibrated to be virtually black, with no shining specks of green anywhere. Once the slide was focused and calibrated, the slide was moved around under the microscope. Several images were taken of different areas of the sample. with the calibrated exposure and gain.

Then, the slide with 40-second irradiation time was placed under the microscope with the same calibrated exposure and gain as the 0-second slide. The slide was then refocused under phase-contrast mode, and then switched back to fluorescence mode. After the sample focused and turned back to fluorescent mode, images of the sample were captured from different areas with the same exposure and gain calibrated for the 0-second slide. The calibration of the exposure and gain should allow the image of the 40-second slide to be very bright, with lots of bright green specks compared to the 0-second slide. The calibration for the exposure and gain required some trial and error between the 0-second and 40-second slides to complete.

After figuring out the exposure and gain, images of the particles that became fluorescent were taken for each slide. When switching slides, each slide was refocused in phase-contrast mode to obtain the best quality images and then changed back to fluorescent mode to take images under the FITC (green) filter. While imaging, like the "0 s" and "40 s" slides, the same steps are repeated – moving the slide around under the microscope for greater focus and capturing images of the fluorescent particles in different regions and areas with the same exposure and gain. These images were finally renamed with their corresponding slide's irradiation time and saved to the computer.

4.5 Image Analysis

Like the image analysis in Experiment 1, the application ImageJ is used to analyze the images taken by the microscope in Experiment 2. Each image taken of the nanoparticles was first imported into the ImageJ software, and then the intensity of the fluorescence of the nanoparticles was analyzed by highlighting each of the particles precisely. This was completed for all the images taken.

Then, from all the data exported from ImageJ, the "mean," the average intensity of the highlighted sections, and "area," the measured value of the highlighted sections, values were kept. Using these two values, the average intensity of the fluorescent particles in the image is calculated by using $\frac{\sum Mean}{\sum Area}$. This is calculated for all the images from the "0 s" irradiation time to the "40 s" irradiation time.

These calculated values for the average intensity of the image were matched with their corresponding image irradiation time in a table, with the irradiation time on the left (independent variable) and the average intensity on the right (dependent variable), in excel to create a graph.

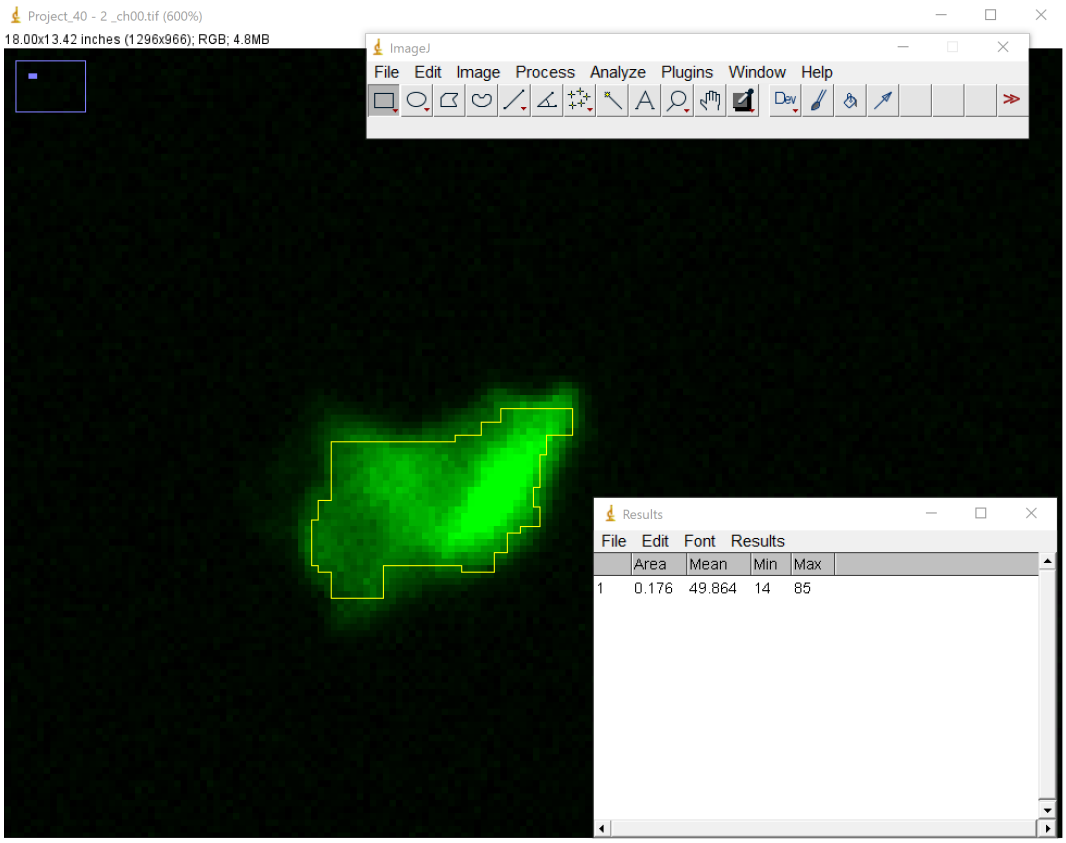

Figure 2: Image J View for Nanoparticles

5. RESULTS

5.1 Experiment 1: Solution of RB in DMSO and DHR

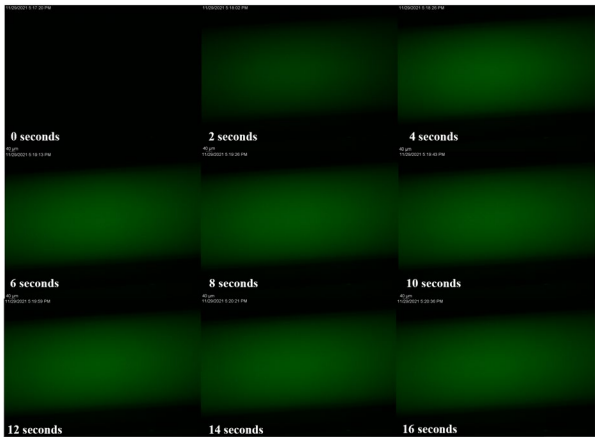

Figure 3: Fluorescence Microscopic Images from Trial 1

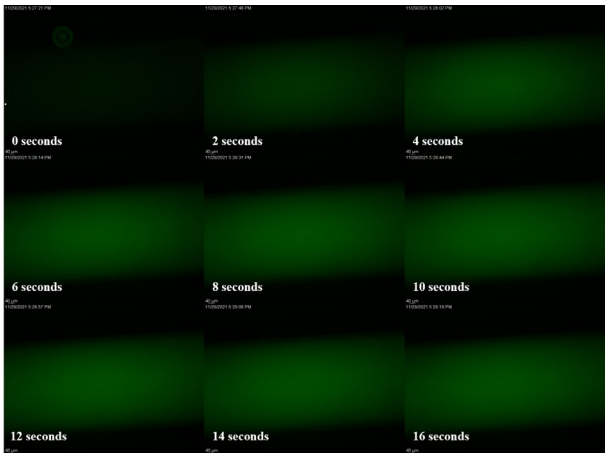

Figure 4: Fluorescence Microscopic Images from Trial 2

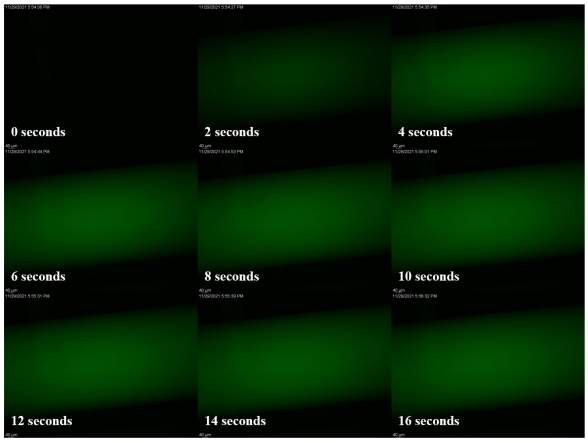

Figure 5: Fluorescence Microscopic Images from Trial 3

Table 1: Table of Fluorescence Intensity Values Measured from ImageJ for RB in DMSO and DHR Images

Time (seconds)	Trial 1	Trial 2	Trial 3
0	0.617	0.718	0.581
2	14.812	12.867	13.796
4	21.972	17.847	20.476
6	22.648	20.507	21.776
8	22.598	21.546	22.881
10	23.725	21.795	23.363
12	24.046	21.800	22.296
14	23.950	22.555	24.053
16	23.992	21.531	23.241

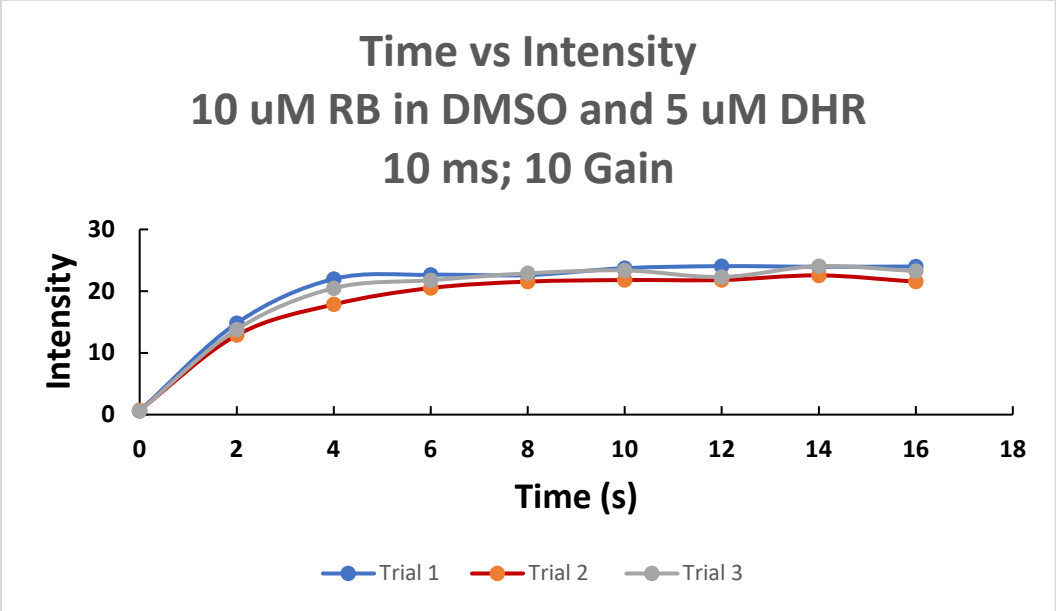

Figure 3: Graph of Time vs Intensity from Experiment 1

Table 2: Table of Fluorescence Intensity Values Measured from ImageJ for Nanoparticle Images

Time (seconds)	Trial 1	Trial 2	Trial 3
0	2.035	2.203	2.232
10	9.498	13.55467	14.83971
20	23.72367	28.969	29.7035
30	41.13675	46.57567	47.4315
40	51.724	51.08271	54.2865

5.2 Experiment 2: Nanoparticles

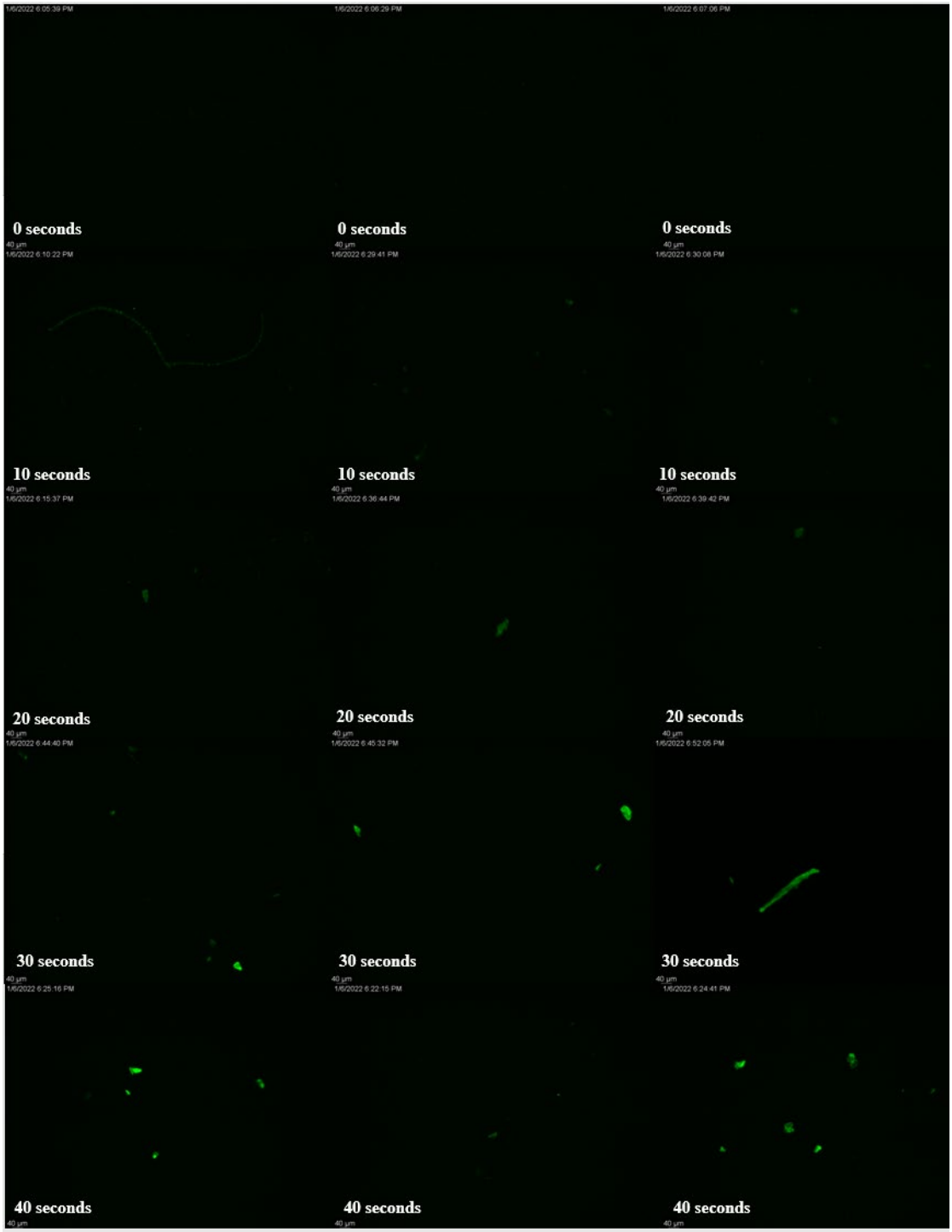

Figure 7: Images from Nanoparticle Experiment

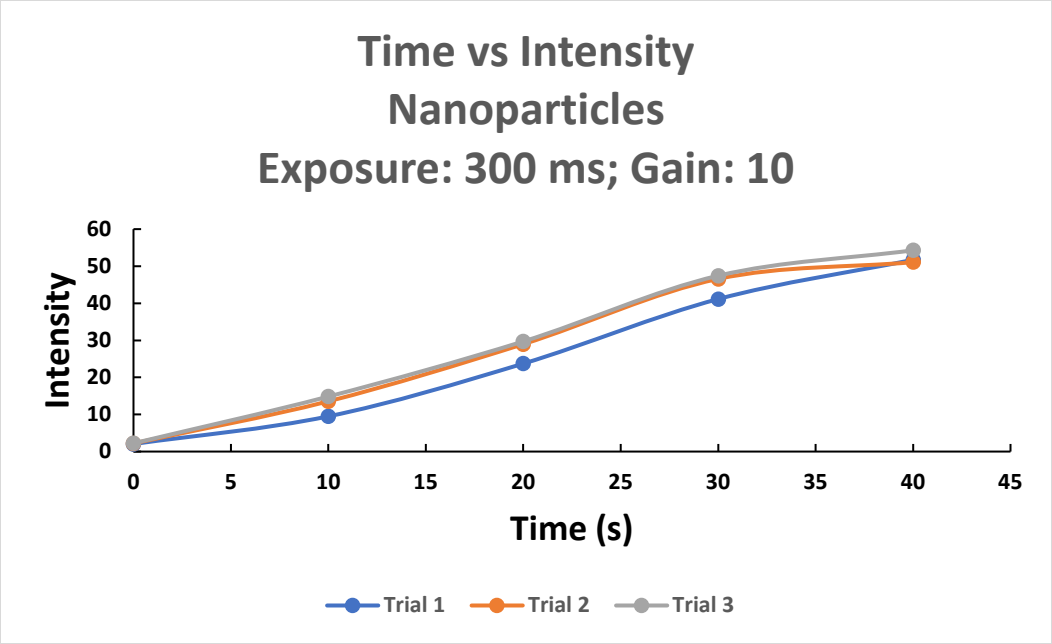

Figure 8: Graph of Time vs Intensity for Experiment 2

6. DISCUSSION AND CONCLUSIONS

6.1 Experiment 1: Solution of RB in DMSO and DHR

The overall trend of the curve in Figure 5, when a solution of RB in DMSO is mixed with DHR and then illuminated to create and detect ROS, exhibits a logarithmic curve. The equation is $y = 0.0646\ln(x) + 21.128$, where y represents intensity and x represents time. For this equation and the data points, R^2 is equal to 0.8462, which indicates 84.62% of the variability in intensity can be explained by this association between intensity of light and time. These results illustrate that this regression exhibits a strong correlation between intensity and time. This in turn indicates that when illuminated under the Texas Red Filter to produce ROS in the sample, and then taken images under the FTC (Green) filter to measure intensity, the curve is seen to first rapidly increase exponentially for about 0 to 4 seconds, and then taper off to a linear, flatter trend with a significantly slower rate of change.

In addition, until the point of saturation at t = 4 seconds, the intensity can be exhibited by a linear curve $y = 4.9738x + 1.6702$, $R^2 = .9701$ or an exponential curve $y = .9223e^{.8906x}$, $R^2 = .7029$, where y represents the intensity and x represents the time. Due to the high R^2 value, which indicates a strong correlation, for both the linear and exponential expressions, the amount of ROS created without limits is shown to increase with longer amounts of illumination time.

6.2 Experiment 2: Nanoparticles

The trend of the curve in Figure 7, with the irradiation of nanoparticles to generate ROS, produces a sigmoidal function The equation of a sigmoidal expression follows $S(x) = \frac{1}{1+e^{-x}}$, where S(x) represents the intensity and x represents time. For this curve in Figure 7, the equation is $y = 2.5065 + \frac{67.2464-2.5065}{1+(\frac{x}{22.5362})^{-2.0753}}$, where y represents intensity and x represents time. This expression justifies the bell-shaped behavior in which the curve is first seen to have a steady rate

of change up till t = 10 seconds, which then becomes an incremental faster rate of change from 10 to 30 seconds, and then again returns to the steady rate of change from 30 to 40 seconds.

Furthermore, the graph can be modeled as a linear curve $y = 1.4853x + 0.5457$, R2 = .9911 or an exponential curve $y = 3.2026e^{0.0991x}$, R2 = 0.9159 until t = 30 seconds, where y represents the intensity and x represents the time. The R2 values of .9911 and .9159 for the linear and exponential expressions respectively, displays that with increasing plasma dose, the amount of ROS created increases as well.

6.3 Final Discussion and Conclusion

Here, two different methods of detecting ROS, during photodynamic therapy, are presented. In the first method a sensor dye DHR is used, which can detect multiple different species of oxidants. This sensor dye was mixed with the photosensitizer Rose Bengal which produces ROS after being illuminated with light ($\lambda = 559\ nm$) and is routinely used for photodynamic therapy. The sensor molecules interact with ROS and its oxidation causes the sample to become fluorescent. Therefore, when the light irradiation time increased, more ROS was created, and hence more ROS was able to oxidize the sensor molecules, causing the overall fluorescence of the samples of increase. This was measured through the intensity of the images through ImageJ and then graphed and analyzed. In the second experiment, nanoparticles containing singlet oxygen sensor dye was used to specifically detect singlet oxygen. Nanoparticles have several advantages over free dye molecules and thus were selected for this application. Singlet oxygen is generated in copious amounts during photodynamic therapy and also plasma therapy. Thus, proof of concept experiments was performed using a plasma source. The amount of singlet oxygen produced is directly proportional to the plasma exposure time, and we observe a steady increase in fluorescence from the nanoparticles as shown in Figure 7.

I conclude that photodynamic therapy can be used to induce ROS production In addition, I also conclude that longer periods of phototherapy induce greater production of ROS and exhibits a linear trend given the higher R^2. This was found based on the linear and exponential models up till the point of saturation for the two experiments. Due to the strong correlation in both experiments for the linear and exponential functions modeling up to the saturation point, it can be seen that the amount of ROS produced by the photosensitizer continues to increase even though the photosensors may not be able to pick them up. The saturation point can be observed at t = 4 seconds for Experiment 1 and t = 30 for Experiment 2.

In addition, after analysis it was found that experiments 1 and 2 exhibited predominantly sigmoidal and liner functions overall, respectively. The saturation curve can be observed in both experimental graphs since the intensity is depicted to rapidly increase until a certain threshold, and then flatten out into a horizontal line, which demonstrates the behavior of an asymptote as well as a carrying capacity limit. In other words, the ROS can only be detected until a certain threshold limit after which the photosensors can no longer reflect the intensity of the increasing light. The slight differences in the shapes of graphs, resulting in the small changes in the expression of the formulas, can also be attributed to the variance between the two different experimental setups and procedures.

However, the amount and type of ROS generated in cells might be very different than those done in a capillary is considered as a limitation to this conclusion. There are some limitations of this technique like sensitivity of the sensor molecule, photobleaching and experimentation on the human which need further experimentation and study.

This data revealed that since the overall intensity of the sample could not be detected past a certain point, the photosensors in the sample had become saturated and reached a threshold experimental limit. Thus, it can be deduced that at this saturation point, the amount of ROS produced in the sample outnumbers the number of photosensors that were present in the sample. However, this can be circumvented by using a higher concentration of sensors. Therefore, I conclude that these fluorescence-based techniques can be extremely useful for quantifying the amount of ROS generated during anti-cancer therapy and therefore aim in therapy optimization and monitoring. This approach will lead to higher therapeutic efficacy and help save countless lives.

ACKNOWLEDGEMENT

I would like to express my deep gratitude to Dr. Aniruddha Ray and Md. Alamgir Kabir for guiding me through this project. This research could not have been completed without their continuous support and guidance. I also wish to show my appreciation to the University of Toledo for allowing me to facilitate their laboratory space, equipment, supplies, and technologies to conduct this research.

REFERENCES

AAT Bioquest, Inc. (2022, January 02). *Quest Graph ™ Four Parameter Logistic (4PL) Curve Calculator*. AAT Bioquest. https://www.aatbio.com/tools/four-parameter-logistic-4pl-curve-regression-online-calculator.

Atenco-Cuautle, J. C., Delgado-López, M. G., Ramos-García, R., Ramírez-San-Juan, J. C., Ramirez-Ramirez, J., & Spezzia-Mazzocco, T. (2019, August 7). *Rose Bengal as a photosensitizer in the photodynamic therapy of breast cancer cell lines*. SPIE Digital Library. Retrieved November 29, 2021, from https://www.spiedigitallibrary.org/conference-proceedings-of-spie/11070/11070A1/Rose-bengal-as-a-photosensitizer-in-the-photodynamic-therapy-of/10.1117/12.2525456.short?SSO=1

Benov, L. (2014, May 10). *Photodynamic therapy: Current status and future directions*. Medical Principles and Practice. Retrieved January 29, 2022, from https://www.karger.com/Article/Fulltext/362416#:~:text=Among%20the%20limitations%20of%20PSs,PDT%20to%20mainly%20superficial%20lesions.

Cancer statistics. National Cancer Institute. (n.d.). Retrieved October 3, 2021, from https://www.cancer.gov/about-cancer/understanding/statistics.

Dihydrorhodamine 123. Thermo Fisher Scientific - US. (n.d.). Retrieved April 24, 2022, from https://www.thermofisher.com/order/catalog/product/D23806#:~:text=Dihydrorhodamine%20123%20is%20an%20uncharged,For%20Research%20Use%20Only.

Dimethyl sulfoxide. American Chemical Society. (n.d.). Retrieved April 24, 2022, from https://www.acs.org/content/acs/en/molecule-of-the-week/archive/d/dimethyl-sulfoxide.html#:~:text=DMSO%20is%20a%20laboratory%20and,used%20solvent%20for%20chemical%20reactions.

Elmore, S. (2007, June). Apoptosis: A review of Programmed Cell Death. Toxicologic pathology. Retrieved October 12, 2021, from https://www.ncbi.nlm.nih.gov/pmc/articles/PMC2117903/.

Gelperina, S., Kisich, K., Iseman, M. D., & Heifets, L. (2005, December 15). The potential advantages of Nanoparticle Drug Delivery Systems in chemotherapy of tuberculosis. American journal of respiratory and critical care medicine. Retrieved November 24, 2021, from https://www.ncbi.nlm.nih.gov/pmc/articles/PMC2718451/#:~:text=The%20important%20technological%20advantages%20of,including%20oral%20application%20and%20inhalation.

Harley, J. C., Suchowerska, N., & McKenzie, D. R. (2020, August). Cancer treatment with gas plasma and with glass plasma-activated liquid: Positives, potentials and problems of clinical translation. Biophysical reviews. Retrieved November 02, 2021, from https://www.ncbi.nlm.nih.gov/pmc/articles/PMC74429664/

Islam, K. M., Anggondowati, T., Deviany, P. E., Ryan, J. E., Fetrick, A., Bagenda, D., Copur, M. S., Tolentino, A., Vaziri, I., McKean, H. A., Dunder, S., Gray, J. E., Huang, C., & Ganti, A. K. (2019). Patient preferences of chemotherapy treatment options and tolerance of chemotherapy side effects in advanced stage lung cancer. BMC Cancer, 19(1), N.PAG. https://doi.org/10.1186/s12885-019-6054-x

Khan, F. A., Akhtar, S. S., & Sheikh, M. K. (2005, January). Cancer treatment - objectives and quality of life issues. The Malaysian journal of medical sciences : MJMS. Retrieved October 4, 2021, from https://www.ncbi.nlm.nih.gov/pmc/articles/PMC3349406/.

MD;, S. M. J. S. I. P. I. B. (n.d.). Fluorescence microscopy. Cold Spring Harbor protocols. Retrieved November 2, 2021, from https://pubmed.ncbi.nlm.nih.gov/25275114/.

Photodynamic therapy (PDT). Cleveland Clinic. (n.d.). Retrieved October 11, 2021, from https://my.clevelandclinic.org/health/treatments/17922-photodynamic-therapy-pdt.

Reactive oxygen species in cancer. Taylor & Francis. (n.d.). Retrieved October 9, 2021, from https://www.tandfonline.com/doi/full/10.3109/10715761003667554.

Photodynamic Therapy for Cancer. National Cancer Institute. (n.d.). Retrieved November 12, 2021, from https://www.cancer.gov/about-cancer/treatment/types/photodynamic-therapy.

Sadat Tabatabaei Mirakabad F;Nejati-Koshki K;Akbarzadeh A;Yamchi MR;Milani M;Zarghami N;Zeighamian V;Rahimzadeh A;Alimohammadi S;Hanifehpour Y;Joo SW; (n.d.). PLGA-based nanoparticles as Cancer Drug Delivery Systems. Asian Pacific journal of cancer prevention: APJCP. Retrieved December 29, 2021, from https://pubmed.ncbi.nlm.nih.gov/24568455/#:~:text=Poly%20(lactic%2Dco%2Dglycolic,biocompatibility%20with%20tissue%20and%20cells.

Sekar, T. V., & Paulmurugan, R. (2014, March 28). Bioluminescence imaging of cancer therapy. Cancer Theranostics. Retrieved October 9, 2021, from https://www.sciencedirect.com/science/article/pii/B9780124077225000062.

Types of cancer treatment. American Cancer Society. (n.d.). Retrieved October 3, 2021, from https://www.cancer.org/treatment/treatments-and-side-effects/treatment-types.html.

Visone, R., & Croce, C. M. (2010, December 16). MIRNAs and cancer. The American Journal of Pathology. Retrieved October 5, 2021, from https://www.sciencedirect.com/science/article/pii/S0002944010609728.

What is cancer? National Cancer Institute. (n.d.). Retrieved October 5, 2021, from https://www.cancer.gov/about-cancer/understanding/what-is-cancer.